

STP 1622, 2021 / available online at www.astm.org / doi: 10.1520/STP162220190029

Ece Alat,¹ Jing Hu,² Douglas E. Wolfe,^{1,3} and Arthur T. Motta^{1,4}

Corrosion and Ion Irradiation Behavior of Ceramic-Coated Nuclear Fuel Cladding



Citation

E. Alat, J. Hu, D. E. Wolfe, and A. T. Motta, "Corrosion and Ion Irradiation Behavior of Ceramic-Coated Nuclear Fuel Cladding," in *Zirconium in the Nuclear Industry: 19th International Symposium*, ed. A. T. Motta and S. K. Yagnik (West Conshohocken, PA: ASTM International, 2021), 149–171. <http://doi.org/10.1520/STP162220190029>⁵

ABSTRACT

Recent concern with fuel safety in accident scenarios has motivated research into accident tolerant fuels (ATF), which are defined as fuels that could increase coping time in case of an accident. This study is an attempt to develop an ATF by improving the corrosion performance of nuclear fuel cladding during a high-temperature excursion through the application of a ceramic coating using physical vapor deposition. In this study, ceramic coatings constituted of single-layer and multi-layer TiN/TiAlN coatings with a titanium bond coat layer to improve adhesion were applied onto ZIRLO sheets using cathodic arc physical vapor deposition. The coating architecture and deposition parameters were systematically optimized to achieve good adhesion and corrosion performance, and an initial evaluation was performed for resistance to radiation damage. The coating performance was highly dependent on coating design architecture, and the best coating architecture was found to be that of eight-layer TiN/TiAlN coatings deposited with optimized parameters. The optimized coatings were

Manuscript received March 6, 2019; accepted for publication January 29, 2020.

¹Dept. of Materials Science and Engineering, The Pennsylvania State University, University Park, PA 16802, USA
E. A.  <https://orcid.org/0000-0003-0312-6269>, A. T. M.  <https://orcid.org/0000-0001-5735-1491>

²Applied Materials Division, IVEM, Building 212, Argonne National Laboratory, Lemont, IL 60439, USA
 <https://orcid.org/0000-0003-1402-5949>

³Applied Research Laboratory, The Pennsylvania State University, 119 Materials Research Building, University Park, PA 16802, USA

⁴Ken and Mary Alice Lindquist Dept. of Nuclear Engineering, The Pennsylvania State University, University Park, PA 16802, USA

⁵ASTM 19th International Symposium on *Zirconium in the Nuclear Industry* on May 19–23, 2019 in Manchester, UK.

Copyright © 2021 by ASTM International, 100 Barr Harbor Drive, PO Box C700, West Conshohocken, PA 19428-2959.

ASTM International is not responsible, as a body, for the statements and opinions expressed in this paper. ASTM International does not endorse any products represented in this paper.

corrosion tested in 360°C water for up to 90 days, showing essentially no oxygen penetration, very low weight gain, and no spallation or debonding. The samples were also examined in microscopy and X-ray diffraction after corrosion testing, and little change was observed. To evaluate the coating performance under irradiation, cross-sectional transmission electron microscopy samples of the coating were subjected to in situ ion irradiation to a dose of 20 dpa with 1 MeV Kr ions at 300°C, followed by further annealing to 800°C. Little interlayer mixing and overall damage accumulation was observed. Coating adhesion was investigated through scratch testing and post-scratched sample failure mode characterization to determine a critical load value for spallation. The coating layers are found to require a high load for debonding and spallation. The results suggest that this optimized coating system is a promising path for developing an ATF.

Keywords

TiN, TiAlN, cladding, coating, accident tolerant fuel, corrosion, irradiation

Introduction

Currently, zirconium (Zr)-based alloys are commonly used as nuclear fuel cladding material in light water reactors because of their desirable properties such as high strength, good corrosion resistance in water at 300°C, and, principally, low neutron absorption cross section.¹⁻³ However, waterside corrosion limits Zr-based alloy cladding service life. Furthermore, during the Fukushima Daiichi accident in 2011, a station blackout significantly impaired reactor cooling, which led to temperature increases in the reactors and accelerated Zr cladding steam oxidation, with significant hydrogen generation.⁴ This resulted in hydrogen explosions in the reactor buildings, which worsened the accident development.⁵⁻⁷

This accident motivated research for alternative nuclear cladding materials to be used as accident tolerant fuels (ATFs) that can provide additional coping time in the case of a loss of coolant accident in a nuclear reactor, thus allowing timely intervention.^{7,8} Different approaches have been proposed to develop protective cladding for ATFs such as the application of protective coating, completely new materials (such as iron-chromium-aluminum [FeCrAl] and silicon carbide [SiC]) and hybrid designs,⁹ and these are reviewed in Terrani.⁹ Among these, the application of coatings on existing Zr-based cladding materials is an eminently practical approach. Various examples of metallic, nonmetallic, oxide, carbide, nitride, and multilayer coating design applications on Zr-based alloys have been proposed.^{1,8,10-43} The present study focuses on developing adherent and enduring multilayer TiN and (Ti,Al)N coatings on Zr-based alloy claddings for enhanced accident tolerance.^{9,44,45}

In developing a coating for nuclear fuel cladding, adhesion of the developed coating to the zirconium-based alloy cladding, coating deposition method scalability to the production size, ease of fabrication, mechanical properties, low neutronic penalty, and maintenance of coating properties under irradiation are the major challenges. The application of transition metal nitride coating can improve material properties such as the wear resistance, chemical inertness, and hardness.⁴⁶

The enhancement of these properties can be adjusted through optimization of the coating composition, coating layer thickness, and coating design architecture. Previous investigations showed that hardness and fracture toughness increase with increasing Al content in the $Ti_{1-x}Al_xN$ coating until $X = 0.6$.^{47–49} Regarding the neutronic properties, coating thicknesses of 10 to 30 μm limit cycle length loss in $Ti_{0.5}Al_{0.5}N$ coatings to only a few days.⁵⁰ Previous studies observed that Argon (Ar+) ion irradiation to ~ 100 dpa causes interlayer mixing in thin-layered AlN/TiN coatings (~ 5 to 10 nm) with indications of TiN grain size growth and the formation of TiAlN layers.^{51–53} Bugnet et al. showed direct current (DC) sputtered and annealed thin films of (Ti,Al)N/Ti₂AlN_x MAX phases to be radiation resistant up to 12 dpa, with no change in either microstructure or crystalline structure.⁵⁴ Studies have also been performed for Cr coatings in which samples were krypton (Kr) ion irradiated to 10 dpa at the interface, showing small changes but good interface and compositional stability after irradiation.⁵⁵

This study uses cathodic arc physical vapor deposition (CA-PVD) to deposit the coatings. This deposition method is a line-of-sight deposition, which provides high ionization and energetic particle bombardment on the substrate surface, leading to good adhesion, dense coating formation, coating microstructure improvement, grain size reduction, microhardness enhancement due to high preferred orientation, and the development of compressive stresses that help blunt cracks, tailorability of the interfacial products (especially in multilayer coatings), and flexibility in cathode and substrate geometry contributing to the scalability to production size and quantities.^{46,56–60} A previous study found less than optimal behavior of TiN and TiAlN coatings, but, as is made clear later in this paper, the coating performance is highly dependent on the coating architecture and deposition parameters, which were quite different in that study.⁴⁵

Physical vapor deposition processes, both cathodic arc and sputter-based techniques, can easily be scaled for high manufacturing throughput and high volume. One method to scale the coating of the tube cladding is to translate the tubes through an annulus composed of the metal (Ti or TiAl) that is evaporated and reacted with nitrogen to form the various nitride-coated layers in a continuous process. The second approach involves using large flat targets positioned a few inches above a series of the rotating tubes to be coated in which the metal species (Ti or TiAl) would be evaporated or sputtered in a nitrogen environment and deposited onto the cladding in a continuous process. Depending on the number of desired coating layers, alternating targets of either titanium or titanium aluminum could be used (i.e., Ti-TiAl-Ti-TiAl) to obtain the desired multilayer design architecture.

One possible concern with CA-PVD is the generation of macrosized metallic particles (1 to 10 μm) that can act as crack initiation sites or form macroparticles on the substrate surface, degrading coating integrity.^{46,61,62}

The aim of this study is to develop corrosion-resistant ceramic coatings that adhere well to ZIRLO substrates and that can withstand the nuclear reactor environment both under normal operation conditions and in the case of a loss-of-coolant accident (LOCA).

Experimental Method

MATERIALS AND COATING

Single-layer $\text{Ti}_{1-x}\text{Al}_x\text{N}$ (where x is ~ 0.50 to 0.67) and multilayer $\text{Ti}_{1-x}\text{Al}_x\text{N}$ (where x is ~ 0.50 to 0.67) and TiN (henceforth referred to as TiAlN or TiN, respectively) coatings were deposited onto ZIRLO corrosion coupons measuring 2.54 cm by 5.08 cm, using CA-PVD. ZIRLO sheets were provided by Westinghouse, with a chemical composition of 1% niobium (Nb), 1% tin (Sn), 300 to 600 wt. ppm Fe and balance Zr. The samples showed the normal texture with preferential orientation of the basal poles close to the normal direction along the transverse plane. As detailed earlier, this study used optimum substrate surface roughness and optimum coating deposition parameters.⁶³ The substrate surface roughness was adjusted to $0.25 \mu\text{m}$ R_a , using SiC paper having 240, 600, and 800 grit, and the substrate surface roughness measurement was performed using a Mitutoyo SJ-201P Surface Roughness Tester. Prior to coating deposition, a 1.6-mm-diameter hole was drilled near one edge of the sample for hanging on an autoclave tree during corrosion tests. The substrate surface was cleaned through 10 min of acetone exposure in an ultrasonic cleaner, deionized water rinse, 10 min of methanol exposure in the ultrasonic cleaner, deionized water rinse, and drying with nitrogen gas.

COATING DEPOSITION

Coatings were deposited using CA-PVD. The dimensions of the PVD chamber were 50.8 cm by 50.8 cm by 50.8 cm. Cylindrical solid cathodes with a diameter of 6.3 cm and a thickness of 3.2 cm were used with two different compositions. One of these was a high-purity (99.999%) elemental titanium dished cylinder used for the titanium bond coating and for the TiN layer deposition. To deposit the TiAlN layer, titanium aluminum cathodes with two different compositions were used: 33at.% Ti–67at.% Al and 20 at.%Ti–80 at.%Al (henceforth coatings deposited with these compositions will be referred to as $\text{Ti}_{33}\text{Al}_{67}\text{N}$ or $\text{Ti}_{20}\text{Al}_{80}\text{N}$, respectively). The pure titanium and the TiAl cathodes were oriented 180° from each other, with the ZIRLO samples located between the cathodes with a spacing of 23 cm. To control the plasma density and location, magnets were placed behind the cathodes.⁶⁴ Shadow bars were placed parallel to the long edges of each sheet substrate at the sample holder to prevent increased coating buildup along the sample edges. The rotating sun/planet system of the deposition chamber could hold eight samples. The radiant heater temperature of the deposition chamber was set to 325°C , as measured by a thermocouple located in close proximity to the samples during deposition. The thermocouple tip was placed in the center of the chamber, parallel to the center of the deposition target (cathode), and in the center of the planetary rotation of the samples. The thermocouple was aligned 5 cm away from the center of each sample in the X – Y direction and with the center of the sample in the Z direction.

The deposition process took place in three main stages: vacuum, ion etching, and coating. During the vacuum stage, the chamber was evacuated to a high vacuum level $< 2.7 \times 10^{-3}$ Pa (2×10^{-5} Torr). Ion etching was then performed to

remove the native oxide from the substrate surface by introducing Ar gas into the chamber and establishing a pressure of 0.7 Pa (5×10^{-3} Torr) while applying a $-1,000$ V bias to the substrate. This was followed by titanium-bond coating (Ti-BC) deposition to enhance adhesion between the substrate and the coating. Ti-BC deposition was performed in an inert argon atmosphere at 1.6 Pa (1.2×10^{-2} Torr) at a substrate bias of -150 V. The Ti-BC layer was deposited to a thickness of ~ 0.6 μm with a deposition rate of 0.75 $\mu\text{m}/\text{min}$. The coating deposition was conducted in a 1.6 Pa N_2 atmosphere, under a $-(50 \text{ to } 75)$ V bias, with an approximate deposition rate of 0.028 $\mu\text{m}/\text{min}$ (1.68 $\mu\text{m}/\text{h}$). The TiN coating layer was deposited through the reaction of the titanium ions arriving on the -150 -V biased substrate surface with the nitrogen atoms in the reactive atmosphere at a 1.6 Pa (1.2×10^{-2} Torr) nitrogen partial pressure. Two coating architectures were investigated in the current study: a single layer TiAlN (to separate the TiAlN layer composition effect from the TiN layer) and the eight-layer TiN/Ti_{1-x}Al_xN. The latter was determined to be the optimum design architecture for enhanced corrosion resistance in a previous study.⁶⁰ The total coating thickness was ~ 10 μm , which for the elements used caused a negligible neutronic penalty relative to uncoated ZIRLO.⁶⁵

SCRATCH TESTING

The adhesion strength of the coatings was examined using scratch testing, according to ASTM C1624, *Standard Test Method for Adhesion Strength and Mechanical Failure Modes of Ceramic Coatings by Quantitative Single Point Scratch Testing*.⁶⁶ The test was performed using a Romulus IV Universal Materials Tester (Spokane, WA, USA). A Rockwell C 200- μm -radius diamond stylus was used to develop a ~ 1 -cm scratch on the coating with a tangential force. Progressive loading with normal force was applied from 0 to 50 N with a 50 N/min rate corresponding to 0.83 N/s. The coating damage was examined using optical microscopy and using scanning electron microscopy (SEM) with energy dispersive spectroscopy (EDS).

CORROSION TESTING

Corrosion testing was performed at Westinghouse in a pure water static autoclave for 90 days at 360°C , with a saturation pressure corresponding to 18.7 MPa at this temperature. The autoclave material was 316 stainless steel. The corrosion tests were performed according to ASTM G2, *Standard Test Method for Corrosion Testing of Products of Zirconium, Hafnium, and Their Alloys in Water at 680°F (360°C) or in Steam at 750°F (400°C)*. Weight gain measurements were performed following the autoclave test as a measure of corrosion. The samples were also examined visually using optical microscopy and SEM.

The structural and morphological properties of samples were further characterized using X-ray diffraction (XRD), and SEM with EDS. Both surface and cross-sectional SEM/EDS analyses were performed. Surface analyses were conducted directly after the autoclave test. Cross-sectional analyses of coated samples were conducted by cutting the samples in half, mounting in cold mount epoxy, grinding, and polishing. XRD studies were conducted on a PANalytical XPert Pro

multipurpose diffractometer instrument with a 240-mm radius, fixed divergence slit (0.25°), receiving slit (0.25°), using copper (Cu) K_α radiation. XRD analyses with grazing incidence (GI) and Bragg-Brentano (BB) scans were performed with a step size of 0.026° two-theta to reveal the phases formed during corrosion. Backscatter and secondary electron (SE) SEM measurements were conducted using an FEI Quanta 200 Environmental SEM at 80 Pa pressure and 20 kV voltage.

IRRADIATION TEST

For the irradiation test, cross-sectional transmission electron microscopy (TEM) samples were prepared using a focused ion beam (FIB) lift out on a ZEISS 540XB FIB with a final low-energy FIB thinning step to ensure that samples were electron transparent for TEM and had a uniform thickness of ~ 100 nm.

In situ ion irradiation on TEM thin foils was performed in the Intermediate Voltage Electron Microscopy facility⁶⁷ at Argonne National Laboratory, which is a Hitachi 9000 microscope operating at 200 keV that is connected to an ion accelerator so that radiation damage can be observed in situ. TEM thin foils were irradiated with 1 MeV Kr ions at a dose rate of 6×10^{11} ions/cm²/sec at 300°C. The fluence was converted to dpa using a Kinchin Pease calculation on the SRIM-2013 code with a 100-nm foil thickness, 1MeV Kr⁺⁺ ions, and displacement energy of 30 eV for Ti, 25 eV for Al, and 28 eV for N.^{68,69} The majority of the ions (more than 97%) were transmitted through the thin foil and, as a result, the damage rate variation in the sample was small ($\sim 15\%$). The final average dpa level on TiAlN/TiN layers was around 20 dpa and ~ 45 dpa on the substrate. The difference was caused by the differences in target masses and in displacement energies. Essentially all the Kr ions penetrated through the thin foil. After irradiation, the samples were annealed in situ to 800°C. Detailed TEM bright field (BF), dark field imaging and diffraction analyses were systematically carried during the irradiation.

Post-irradiated samples were studied using a FEI-Talos microscope at the Center for Nanoscale Materials at Argonne National Laboratory. The microstructure and microchemistry of the samples were examined by TEM, scanning transmission electron microscope, and energy dispersive X ray, which provide a complementary view of the samples including the shape, size, and crystallographic texture of grains in the ZIRLO substrate and coatings, the particles, cracking, nanoscale porosity, and the local chemistry of the coating-bonding-substrate interface.

Results and Discussion

AS-DEPOSITED COATING

During plasma deposition, TiAlN is deposited as a metastable phase and the cathode composition is one of the parameters that dictates the amount of aluminum atoms that replace the titanium atoms.^{46,70} Table 1 shows the elemental analysis data in atomic percent and weight percent of the single-layer Ti₃₃Al₆₇N coating and the Ti₂₀Al₈₀N coating. Because the cathode composition controls the coating

TABLE 1 Composition of TiAlN coatings deposited using cathodes having 33 at.% Ti-67 at.% Al and 20 at.% Ti-80 at. Al

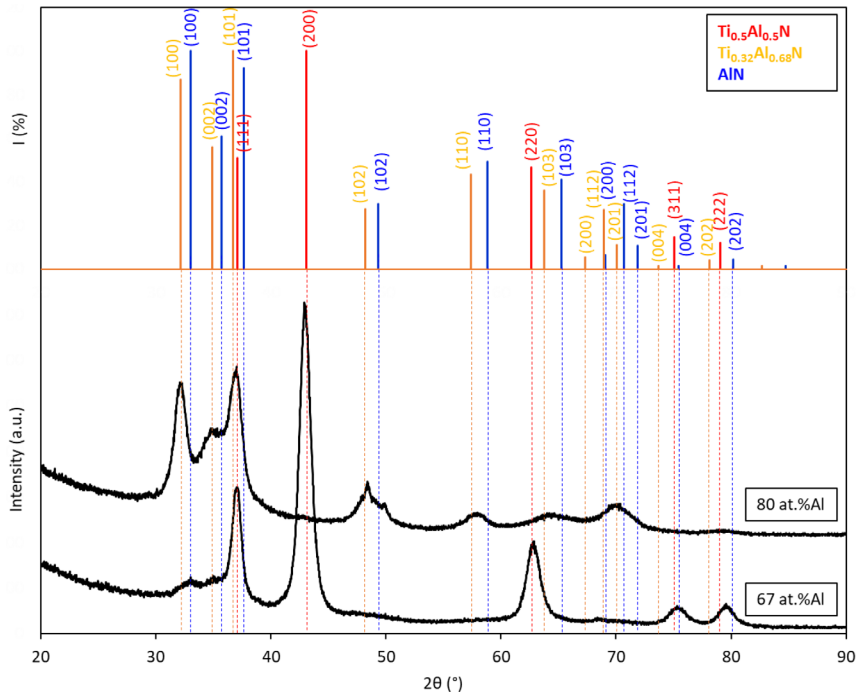
Cathode Composition	Ti, at.%	Al, at.%	N, at.%	Ti, wt.%	Al, wt.%	N, wt.%
33 at.% Ti-67 at.% Al	13.10 ± 0.47	25.83 ± 0.60	59.68 ± 2.34	28.71 ± 0.77	31.90 ± 0.54	38.26 ± 1.51
20 at.% Ti-80 at.% Al	8.76 ± 0.20	32.98 ± 0.34	58.26 ± 0.50	19.73 ± 0.36	41.85 ± 0.29	38.39 ± 0.50

Note: Coating compositions were determined using EDS point analysis.

composition, the Al/Ti ratio of $Ti_{33}Al_{67}N$ was ~ 2 and Al/Ti ratio of $Ti_{20}Al_{80}N$ coating was ~ 4 , as expected.

To identify the phases in the coatings, grazing incidence x-ray diffraction (GIXRD) was performed at a 1° incident angle. The overlapped XRD patterns of the $Ti_{33}Al_{67}N$ and $Ti_{20}Al_{80}N$ coatings are presented in [figure 1](#). The $Ti_{33}Al_{67}N$ coating

FIG. 1 GIXRD measurement patterns of coatings deposited with cathodes having a composition of 33 at.% Ti-67 at.% Al and 20 at.% Ti-80 at.% Al. GIXRD was performed using a $Cu-K_\alpha$ (1.54048 Å) radiation and with a grazing incidence angle of 1° .



phase was identified to be $\text{Ti}_{0.5}\text{Al}_{0.5}\text{N}$ (ICDD PDF# 04-005-5251), which has a cubic crystal structure. The $\text{Ti}_{20}\text{Al}_{80}\text{N}$ coating peak patterns were fitted as the $\text{Ti}_{0.32}\text{Al}_{0.68}\text{N}$ phase (ICDD-PDF# 04-017-4686) and AlN (ICDD PDF# 04-004-4544), which have hexagonal crystal structures. The difference between the two patterns can easily be observed from the (200) peak of the $\text{Ti}_{0.5}\text{Al}_{0.5}\text{N}$ phase at 43.14° , which is not observed in the case of the $\text{Ti}_{0.32}\text{Al}_{0.68}\text{N}$ phase pattern. Broad peaks appeared, suggesting an amorphous or nanocrystalline composite coating structure. This broadening was more pronounced for coatings deposited with $\text{Ti}_{20}\text{Al}_{80}\text{N}$ coating, indicating an increased nanocrystalline composite structure. However, there was peak shifting toward lower 2θ angles relative to the PDF values (higher d-spacing), which is attributed to the compressive strains in the normal direction but with elongation parallel to the coating surface due to Poisson's ratio.⁷¹ Further analysis performed with TEM during irradiation analysis will be presented later in this manuscript.

Figure 2 shows surface SEM images of single-layer $\text{Ti}_{33}\text{Al}_{67}\text{N}$ and $\text{Ti}_{20}\text{Al}_{80}\text{N}$ coatings. The $\text{Ti}_{20}\text{Al}_{80}\text{N}$ coating layer exhibited a greater density of surface macro-particles compared to the $\text{Ti}_{33}\text{Al}_{67}\text{N}$ coating, likely because of its higher Al content.⁷² Figure 3 shows the cross-sectional SEM-BSE images of the $\text{Ti}_{33}\text{Al}_{67}\text{N}$ and $\text{Ti}_{20}\text{Al}_{80}\text{N}$ coatings. The cross-sectional image shows the ZIRLO substrate and titanium bond coating, and it demonstrates that the eight TiN and TiAlN layers of the coatings were deposited uniformly. Compositional analysis showed uniform content of Ti, Al, and N in the respective layers and no ingress of these alloying elements onto the metal substrate.

SCRATCH TESTING

Figure 4 shows SEM images of single-layer $\text{Ti}_{33}\text{Al}_{67}\text{N}$ and $\text{Ti}_{20}\text{Al}_{80}\text{N}$ coating samples on which scratch testing was performed. The $\text{Ti}_{33}\text{Al}_{67}\text{N}$ coating did not show gross spallation up to the maximum load of 50 N, while coating gross spallation initiated in the $\text{Ti}_{20}\text{Al}_{80}\text{N}$ at 41.7 N, indicating that this coating is less adherent to the substrate than $\text{Ti}_{33}\text{Al}_{67}\text{N}$. This is attributed to a combination of high residual stress within the

FIG. 2 Surface SEM SE images of coatings deposited by using cathodes having 33 at.% Ti-67 at.% Al (A) and 20 at.% Ti-80 at.% Al (B).

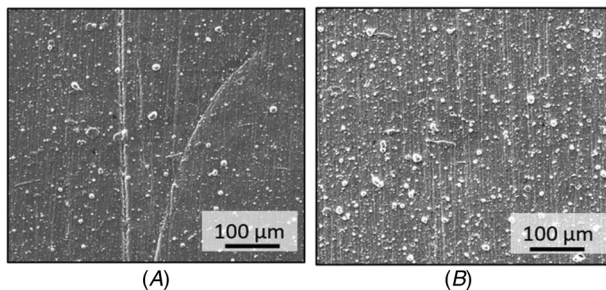


FIG. 3 Cross-sectional SEM-backscattered electron (BSE) images of coatings deposited using cathodes with 33 at.% Ti-67 at.% Al (A) and 20 at.% Ti-0 at.% Al (B).

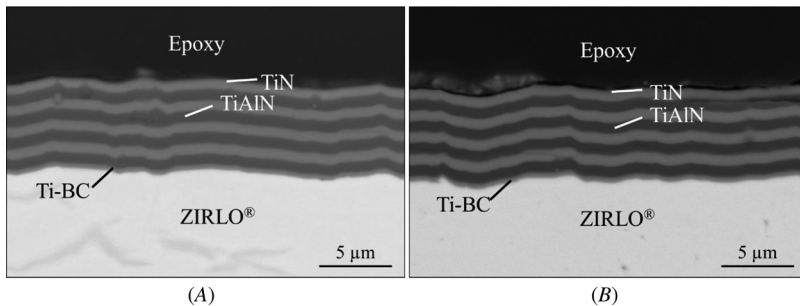
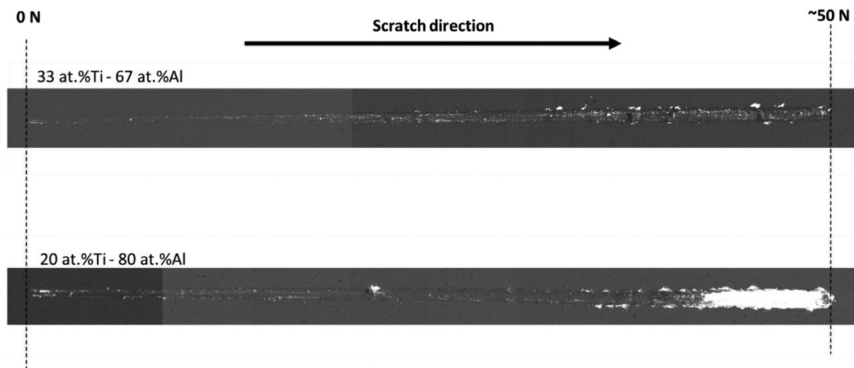


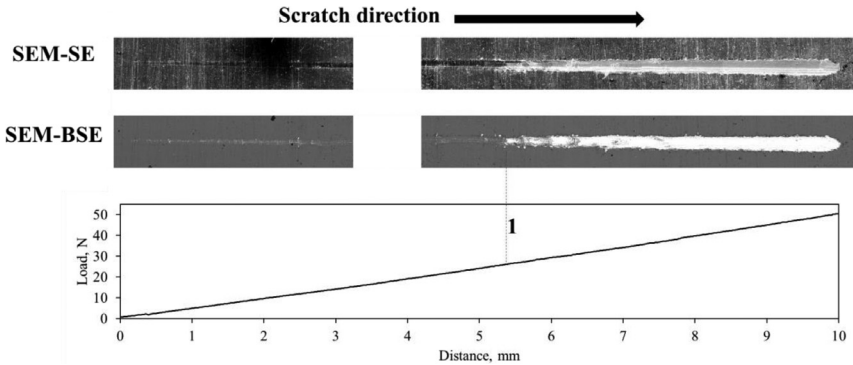
FIG. 4 SEM-BSE image of scratched TiAlN coatings deposited with 50 V substrate bias, 60 A source current, and using a cathode either with 33 at.% Ti-67 at.% Al or 20 at.% Ti-80 at.% Al.



coating and an increased hardness difference between the $\text{Ti}_{20}\text{Al}_{80}\text{N}$ coating and the ZIRLO substrate that resulted in a decrease in the adhesion critical load.⁷³ Another possible contributor could be differences in surface roughness between the two different coatings resulting from different rates of macroparticle formation.^{72,74,75}

The eight-layer TiN/TiAlN coatings with $\text{Ti}_{33}\text{Al}_{67}\text{N}$ and $\text{Ti}_{20}\text{Al}_{80}\text{N}$ showed gross spallation at ~ 27 N and ~ 26 N, respectively. Figure 5 shows SEM SE, SEM-BSE images of the scratch and the corresponding load-distance data of the eight-layer TiN/ $\text{Ti}_{20}\text{Al}_{80}\text{N}$ -coated ZIRLO sheet. It can be concluded that cathode composition variation did not affect coating adhesion significantly in the case of select deposition parameters. The fact that multilayer coatings require lower critical load for gross spallation can be connected to the thinner layers present in the case of multilayer coatings.⁷⁶

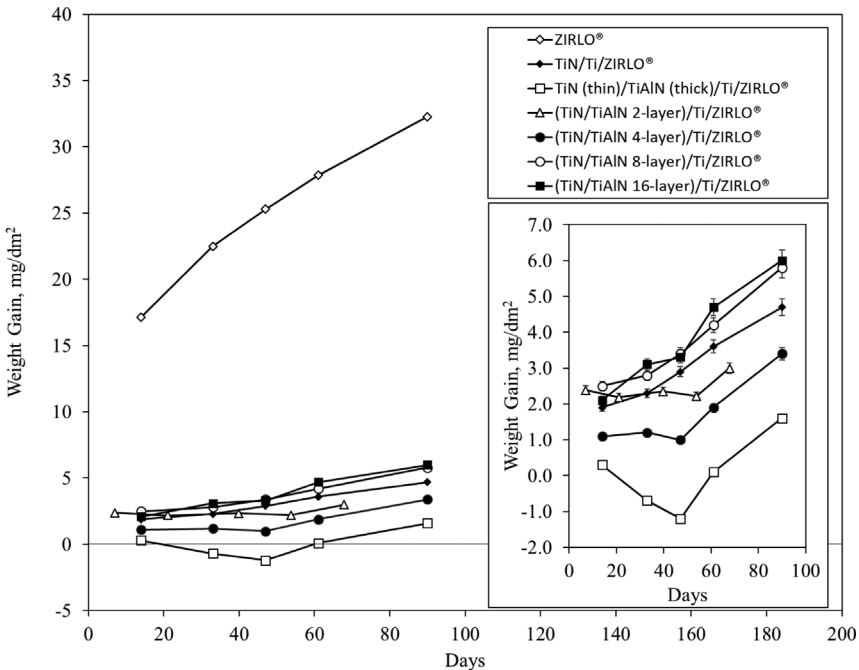
FIG. 5 The scratch test result of the eight-layer TiN/Ti₂₀Al₈₀N/Ti/ZIRLO sheet.



CORROSION TESTS

As long as no oxide spalling or dissolution occurs, weight gain analysis is a valid method to evaluate zirconium oxidation. Figure 6 shows results of previous studies⁶⁴

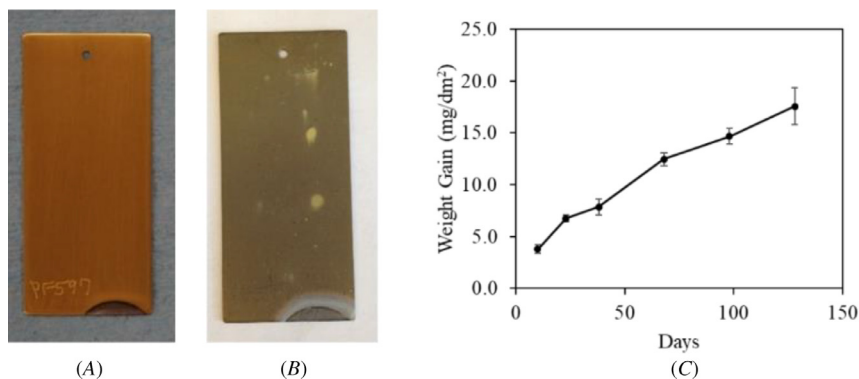
FIG. 6 Weight gain (mg/dm²) as a function of exposure time (days) for samples tested in autoclave at 360°C and 18.7 MPa up to 89 days. Multilayer design architectures showed better corrosion resistance compared to uncoated ZIRLO.⁶⁴



in which various multilayer coating architectures were tested during autoclave corrosion, and the weight gain for each coating design was determined to evaluate the coating design architecture corrosion performance. In addition to the weight gain, the retention of the coating (no spallation or delamination) was also evaluated; one of the samples showed weight loss, indicating spallation, so that was evaluated as a poor performing sample. Contrary to what was stated in Brachet et al.,⁴⁴ no weight loss and thus no loss of Al was observed in the well-performing samples, and thus their overall conclusion as to the unsuitability of TiAlN coatings is without basis. The eight-layer TiN/TiAlN coating design, having TiAlN layers deposited using 33at%Ti–67 at.%Al cathode, showed the lowest weight gain and no coating spallation or delamination.

This study has evaluated the corrosion performance of an eight-layer TiN/TiAlN coating having a TiAlN layer deposited by using 20 at.%Ti–80 at.% Al cathode. **Figure 7A** shows a digital image of the as-deposited coating with gold-colored TiN as the top layer. **Figure 7B** shows a picture of the same sample after 23 days of autoclave corrosion testing. The sample shows a small degree of discoloration due to corrosion but no visible spallation/delamination of the coating. In this case, the autoclave test was continued up to 128 days and the weight gain data are shown in **figure 7C**. Visual analysis confirmed that no spallation of the coating occurred after the 128-day exposure. After 90 days of autoclave testing, the weight gain was ~ 15 mg/dm², which is two times more than the weight gain observed in the case of the eight-layer TiN/TiAlN coating design having TiAlN layers deposited using 33at%Ti–67 at.%Al cathode but half of the uncoated ZIRLO sample weight gain. The reason for the higher weight gain (**fig. 7C**) in the case of the Ti₂₀Al₈₀N coating compared to that of the Ti₃₃Al₆₇N sample is not clear. Although its hexagonal

FIG. 7 (A) Digital image of as-deposited, (B) digital image of 23 days' autoclave-tested, and (C) weight gain data of 128 days' autoclave-tested eight-layer TiN/TiAlN-coated ZIRLO sheet.

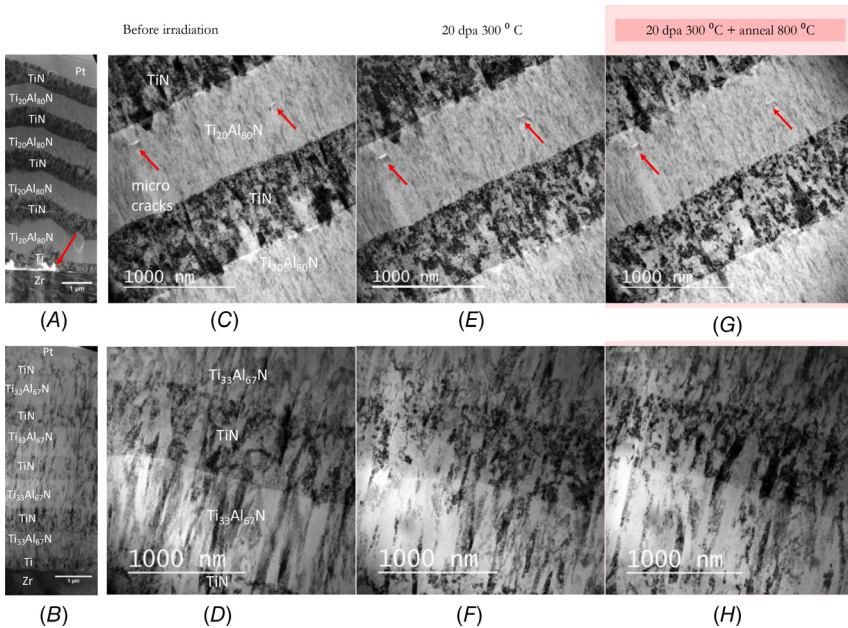


crystal structure with increased aluminum content can degrade corrosion performance,^{46,77} the outer layer in each case is TiN.

IRRADIATION TESTS

The in situ ion irradiation experiments of coating samples with 1 MeV Kr ions showed good irradiation resistance of the coatings (fig. 8A-3 and B-3). The coatings retained their integrity after irradiation to a dose of 20 dpa at 300°C. No irradiation defects above 1 nm and no obvious changes in the existing columnar grain structure and size were observed. In particular, microcracks present in the Ti₂₀Al₈₀N layer in Sample A before irradiation (arrowed in fig. 8A) did not grow under irradiation. No evidence of layer intermixing was observed after ion irradiation. The interface remains sharp and distinct with no signs of intermixing of the layers. Diffraction patterns from the TiN layers showed no diffuse rings after irradiation, indicating no amorphization has occurred, which is in agreement with a previous finding involving nanocrystalline TiN ceramics.⁷⁸ The nanolayer structure within the TiAlN layer also remains during the irradiation, indicating that there is no mixing of layers.

FIG. 8 TEM-BF images of Sample A (Ti₂₀Al₈₀N + TiN) and Sample B (Ti₃₃Al₆₇N + TiN): (A, B) overview of coatings before irradiation, (C, D) higher magnified images showing TiN and TiAlN layers before irradiation, (E, F) after 20 dpa/300°C ion irradiation, and (G, H) after 20 dpa/300°C ion irradiation plus anneal at 800°C.

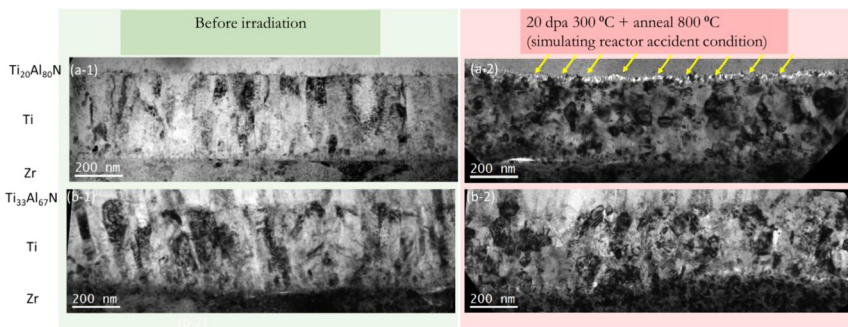


After ion irradiation, the samples were annealed in situ to 800°C for 30 min to mirror a reactor-accident condition. No irradiation defects above 1 nm and no obvious changes in existing columnar grain structure and size were observed after annealing. The cracks and voids did not grow, and coating layers remained intact, as shown in [figure 8A-4](#) and [B-4](#).

The remarkable radiation resistance of the coating layers can be explained in several ways. First, thermodynamically, TiN and AlN have a positive heat of mixing (i.e., they are immiscible), so no chemical driving force is present for intermixing of these two layers. Second, the very fine columnar microstructure in both TiAlN and TiN layers created by the CA-PVD process provides a high density of grain boundaries that could act as effective defect sinks and recombination centers. Third, the interfaces in the nanolayered structure also help to increase the sink density. In this material, nanolayers of TiN and AlN within the TiAlN layers are present with a dimension of around 5 to 10 nm, which is likely to be above the critical thickness for intermixing, as reported in the literature.⁷⁹ At an elevated temperature of around 900°C, spinodal decomposition of TiAlN into TiN and AlN was observed using an in situ X-ray study.⁸⁰ However, in that case, because the TiAlN layer had already decomposed during the PVD process, no phase transformation occurred.

Although no change was seen in the layers themselves, in one of the samples, some change was observed in the bond coat layer. As mentioned previously, between the Zr matrix and the first TiAlN layer, a thin layer of Ti was deposited as the bonding layer to increase the coating adhesion to the matrix and to redistribute the compressive stress at the interface.^{81,82} The thickness of the Ti layer is approximately 350 nm, and the columnar grain size is around 30 to 50 nm wide and 300 nm long ([fig. 9](#)). There are obvious differences between the two samples after annealing. In the Ti₂₀Al₈₀N layer sample, a 20-nm-thick void layer developed at the

FIG. 9 TEM-BF images of coating/Zr matrix interface microstructure of Sample A (Ti₂₀Al₈₀N + TiN) and Sample B (Ti₃₃Al₆₇N + TiN): (A-1)(B-1) before irradiation overview, and (A-2) (B-2) after 20 dpa ion irradiation and 800°C anneal. Note the void layer is highlighted by the arrows in (A-2).



interface of the Ti bond coat layer and the first $\text{Ti}_{20}\text{Al}_{80}\text{N}$ layer, which could lead to a potential failure by coating delamination. At elevated temperature, the interface becomes a vacancy sink and, after 30 min, vacancies accumulate into a layer of porosity. However, this does not occur in the $\text{Ti}_{33}\text{Al}_{67}\text{N}$ sample.

Overall, the preliminary results of the response of the material to radiation damage after 20 dpa followed by high-temperature anneal was encouraging: no changes were seen in the multilayers and the optimized sample composition also showed no changes to the bond coating. The current results are preliminary, however, and although they are promising, among other issues the resistance of these coatings to cracking and spallation during high-temperature excursions (also involving ballooning) needs to be demonstrated.

Conclusions

In this study, single-layer TiAlN and eight-layer TiN/TiAlN coatings deposited on ZIRLO corrosion coupons using cathodic arc physical vapor deposition were tested for corrosion resistance and resistance to radiation damage with a view to developing an ATF coating. TiAlN layers deposited with either 33at.%Ti–67 at.%Al and 20 at.%Ti–80 at.%Al cathodes, and the coating performance deposited with these two different composition cathodes was evaluated considering adhesion, corrosion, and irradiation.

Key observations were as follows:

1. The coating performance depended strongly on deposition parameters. Previously identified optimized parameters for layer deposition were:
 - a. Substrate surface roughness ($0.25 \mu\text{m} R_a$)
 - b. Titanium bond coating thickness ($0.6 \mu\text{m}$)
 - c. Substrate bias (-50 V)
 - d. Nitrogen partial pressure (1.6 Pa)
 - e. Multilayer design (eight-layer) with an overall layer thickness of about $10 \mu\text{m}$.

With these parameters, coating adhesion and corrosion performance were optimized.

2. Coated samples were corrosion tested in an autoclave at 360°C for 89 to 128 days and showed essentially no oxygen ingress and no spallation or delamination. The $\text{Ti}_{33}\text{Al}_{67}\text{N}$ showed better corrosion performance in the autoclave than $\text{Ti}_{20}\text{Al}_{80}\text{N}$.
3. In situ ion irradiation of both samples on the coatings showed good irradiation resistance of the coatings. After irradiation to 20 dpa followed by anneal at 800°C , no irradiation defects above 1 nm during irradiation were observed and no obvious change in the existing coating's columnar grain structure and size were detected.

Although these results are encouraging, much more research and development still need to be performed to ensure that such coatings are stable in the reactor

environment for the exposures required. However, one advantage of physical vapor deposition coating is that it is relatively straightforward to scale it up to industrial manufacturing, raising the possibility that it can be developed for practical applications.

ACKNOWLEDGMENTS

The authors would like to thank Pete Baldo and Ed Ryan at the Argonne National Laboratory for their help during the experiment. This work was supported by the U.S. Department of Energy (DOE), Office of Nuclear Energy under DOE Idaho Operations Office Contract DE-AC07-051D14517 as part of a Nuclear Science User Facilities experiment. Use of the Center for Nanoscale Materials, an Office of Science user facility, was supported by the DOE, Office of Science, Office of Basic Energy Sciences, under Contract No. DE-AC02-06CH11357.

References

1. Z. Duan, H. Yang, Y. Satoh, K. Murakami, S. Kano, Z. Zhao, J. Shen, and H. Abe, "Current Status of Materials Development of Nuclear Fuel Cladding Tubes for Light Water Reactors," *Nuclear Engineering and Design* 316 (2017): 131–150, <https://doi.org/10.1016/j.nucengdes.2017.02.031>
2. R. Krishnan and M. K. Asundi, "Zirconium Alloys in Nuclear Technology," *Proceedings of the Indian Academy of Sciences Section C: Engineering Sciences* 4 (1981): 41–56.
3. T. R. Allen, R. J. M. Konings, and A. T. Motta, "Corrosion of Zirconium Alloys," *Comprehensive Nuclear Materials* 5 (2012): 49–68, <https://doi.org/10.1016/B978-0-08-056033-5.00063-X>
4. K. A. Terrani, S. J. Zinkle, and L. L. Snead, "Advanced Oxidation-Resistant Iron-Based Alloys for LWR Fuel Cladding," *Journal of Nuclear Materials* 448 (2014): 420–435, <https://doi.org/10.1016/j.jnucmat.2013.06.041>
5. N. P. Neureiter, B. J. Garrick, R. A. Bari, J. Beard, M. Percy, M. Q. Brewster, M. L. Corradini, et al., *Lessons Learned from the Fukushima Nuclear Accident for Improving Safety of U.S. Nuclear Plants* (Washington, DC: The National Academy of Sciences, 2014).
6. Tokyo Electric Power Company, Inc., *Fukushima Nuclear Accident Analysis Report*, June 2012.
7. S. Bragg-Sitton, "Development of Advanced Accident-Tolerant Fuels for Commercial LWRs," *Nuclear News* 57, no. 3 (2014): 83–91.
8. K. Barrett, S. Bragg-Sitton, and D. Galicki, *Advanced LWR Nuclear Fuel Cladding System Development Trade-Off Study*, Report Number: INL/Ext-12-27090 (Idaho Falls, ID: Idaho National Laboratory, 2012).
9. K. A. Terrani, "Accident Tolerant Fuel Cladding Development: Promise, Status, and Challenges," *Journal of Nuclear Materials* 501 (2018): 13–30.
10. C. K. Ang, K. Terrani, J. Burns, and Y. Katoh, *Examination of Hybrid Metal Coatings for Mitigation of Fission Product Release and Corrosion Protection of LWR SiC/SiC*, ORNL/TM-2016/332, (Oak Ridge, TN: Oak Ridge National Laboratory, 2016).
11. K. Hauffe and V. Martinez, "Oxidation and Corrosion of Tin-Coated Zircaloy-4," *Journal of the Electrochemical Society* 123 (1976): 595–602, <https://doi.org/10.1149/1.2132892>
12. S. V. Ivanova, E. M. Glagovsky, K. Y. Nikonorov, I. I. Belugin, and I. A. Khazov, "Methods to Increase Corrosion Stability and Wear Resistance of LWR Active Core Zirconium

- Components during Operation and in Conditions of Loss-of-Coolant Accident,” in *Proceedings of Top Fuel 2013* (LaGrange Park, IL: American Nuclear Society, 2013), 334–350.
13. H.-G. Kim, I.-H. Kim, Y.-I. Jung, D.-J. Park, J.-Y. Park, and Y.-H. Koo, “High-Temperature Oxidation Behavior of Cr-Coated Zirconium Alloy,” in *Proceedings of Top Fuel 2013* (LaGrange Park, IL: American Nuclear Society, 2013), 842–846.
 14. J.-H. Park, H.-G. Kim, J. Park, Y.-I. Jung, D.-J. Park, and Y.-H. Koo, “High Temperature Steam-Oxidation Behavior of Arc Ion Plated Cr Coatings for Accident Tolerant Fuel Claddings,” *Surface and Coatings Technology* 280 (2015): 256–259, <https://doi.org/10.1016/j.surfcoat.2015.09.022>
 15. H.-G. Kim, I.-H. Kim, Y.-I. Jung, D.-J. Park, J.-Y. Park, and Y.-H. Koo, “Adhesion Property and High-Temperature Oxidation Behavior of Cr-Coated Zircaloy-4 Cladding Tube Prepared by 3D Laser Coating,” *Journal of Nuclear Materials* 465 (2015): 531–539, <https://doi.org/10.1016/j.jnucmat.2015.06.030>
 16. H.-G. Kim, J.-H. Yang, W. J. Kim, and Y.-H. Koo, “Development Status of Accident-Tolerant Fuel for Light Water Reactors in Korea,” *Nuclear Engineering and Technology* 48 (2016): 1–15, <https://doi.org/10.1016/j.net.2015.11.011>
 17. D.-J. Park, H.-G. Kim, Y.-I. Jung, J.-H. Park, J.-H. Yang, and Y.-H. Koo, “Behavior of an Improved Zr Fuel Cladding with Oxidation Resistant Coating under Loss-of-Coolant Accident Conditions,” *Journal of Nuclear Materials* 482 (2016): 75–82, <https://doi.org/10.1016/j.jnucmat.2016.10.021>
 18. J. Carr, G. Vasudevamurthy, L. Snead, B. Hinderliter, and C. Massey, “Investigations of Aluminum-Doped Self-Healing Zircaloy Surfaces in Context of Accident-Tolerant Fuel Cladding Research,” *Journal of Materials Engineering and Performance* 25 (2016): 2347–2355, <https://doi.org/10.1007/s11665-016-2094-4>
 19. W. G. Luscher, E. R. Gilbert, S. G. Pitman, and E. F. Love, “Surface Modification of Zircaloy-4 Substrates with Nickel Zirconium Intermetallics,” *Journal of Nuclear Materials* 433 (2013): 514–522, <https://doi.org/10.1016/j.jnucmat.2012.05.039>
 20. K. A. Terrani, C. M. Parish, D. Shin, and B. A. Pint, “Protection of Zirconium by Alumina- and Chromia-Forming Iron Alloys under High-Temperature Steam Exposure,” *Journal of Nuclear Materials* 438 (2013): 64–71, <https://doi.org/10.1016/j.jnucmat.2013.03.006>
 21. C. Tang, M. Stueber, H. J. Seifert, and M. Steinbrueck, “Protective Coatings on Zirconium-Based Alloys as Accident-Tolerant Fuel (ATF) Claddings,” *Corrosion Reviews* 35, no. 3 (2017): 141–165, <https://doi.org/10.1515/correv-2017-0010>
 22. W. Zhong, P. A. Mouche, X. Han, B. J. Heuser, K. K. Mandapaka, and G. S. Was, “Performance of Iron-Chromium-Aluminum Alloy Surface Coatings on Zircaloy 2 under High-Temperature Steam and Normal BWR Operating Conditions,” *Journal of Nuclear Materials* 470 (2016): 327–338, <https://doi.org/10.1016/j.jnucmat.2015.11.037>
 23. R. H. Baney and J. S. Tulenko, *An Innovative Ceramic Corrosion Protection System for Zircaloy Cladding*, Revised Project Summary and 4th Quarter Report, NERI Research Project No. 4508230-12, FG03-99SF21882 (Gainesville: University of Florida, 2000).
 24. Y. Al-Olayyan, G. E. Fuchs, R. Baney, and J. Tulenko, “The Effect of Zircaloy-4 Substrate Surface Condition on the Adhesion Strength and Corrosion of SiC Coatings,” *Journal of Nuclear Materials* 346 (2005): 109–119, <https://doi.org/10.1016/j.jnucmat.2005.05.016>
 25. B. R. Maier, B. L. Garcia-Diaz, B. Hauch, L. C. Olson, R. L. Sindelar, and K. Sridharan, “Cold Spray Deposition of Ti₂AlC Coatings for Improved Nuclear Fuel Cladding,” *Journal of Nuclear Materials* 466 (2015): 1–6, <https://doi.org/10.1016/j.jnucmat.2015.06.028>
 26. H. Yeom, B. Hauch, G. Cao, B. Garcia-Diaz, M. Martinez-Rodriguez, H. Colon-Mercado, L. Olson, and K. Sridharan, “Laser Surface Annealing and Characterization of Ti₂AlC Plasma Vapor Deposition Coating on Zirconium-Alloy Substrate,” *Thin Solid Films* 615 (2016): 202–209, <https://doi.org/10.1016/j.tsf.2016.07.024>

27. D. A. Roberts, "Magnetron Sputtering and Corrosion of Ti-Al-C and Cr-Al-C Coatings for Zr-Alloy Nuclear Fuel Cladding" (master's thesis, The University of Tennessee, 2016).
28. J. H. Sung, T. H. Kim, and S. S. Kim, "Fretting Damage of TiN Coated Zircaloy-4 Tube," *Wear* 250 (2001): 658–664, [https://doi.org/10.1016/S0043-1648\(01\)00674-3](https://doi.org/10.1016/S0043-1648(01)00674-3)
29. F. Khatkhatay, L. Jiao, J. Jian, W. Zhang, Z. Jiao, J. Gan, H. Zhang, X. Zhang, and H. Wang, "Superior Corrosion Resistance Properties of TiN-Based Coatings on Zircaloy Tubes in Supercritical Water," *Journal of Nuclear Materials* 451 (2014): 346–351, <https://doi.org/10.1016/j.jnucmat.2014.04.010>
30. K. T. Kim, K. Park, J. Y. Park, and S. Noh, "The Effect of a Ceramic Coating on Zr Alloys in Terms of Corrosion," *Transactions of the Korean Nuclear Society Spring Meeting* (2013): 30–31.
31. K. Daub, R. Van Nieuwenhove, and H. Nordin, "Investigation of the Impact of Coatings on Corrosion and Hydrogen Uptake of Zircaloy-4," *Journal of Nuclear Materials* 467 (2015): 260–270, <https://doi.org/10.1016/j.jnucmat.2015.09.041>
32. K. Sridharan, S. P. Harrington, A. K. Johnson, J. R. Licht, M. H. Anderson, and T. R. Allen, "Oxidation of Plasma Surface Modified Zirconium Alloy in Pressurized High Temperature Water," *Materials & Design* 28, no. 4 (2007): 1177–1185, <https://doi.org/10.1016/j.matdes.2006.01.019>
33. D. Jin, F. Yang, Z. Zou, L. Gu, X. Zhao, F. Guo, and P. Xiao, "A Study of the Zirconium Alloy Protection by Cr₃C₂-NiCr Coating for Nuclear Reactor Application," *Surface and Coatings Technology* 287 (2016): 55–60, <https://doi.org/10.1016/j.surfcoat.2015.12.088>
34. S. T. Park, "Amorphous Alumina Oxidation Protective Coatings for Zircaloy Based on a Compositional Gradient Layer System" (PhD diss., University of Florida, 2004).
35. A. S. Kuprin, V. A. Belous, V. N. Voyevodin, V. V. Bryk, R. L. Vasilenko, V. D. Ovcharenko, E. N. Reshetnyak, G. N. Tolmachova, and P. N. V'yugov, "Vacuum-Arc Chromium-Based Coatings for Protection of Zirconium Alloys from the High-Temperature Oxidation in Air," *Journal of Nuclear Materials* 465 (2015): 400–406, <https://doi.org/10.1016/j.jnucmat.2015.06.016>
36. A. S. Kuprin, V. A. Belous, V. N. Voyevodin, V. V. Bryk, R. L. Vasilenko, V. D. Ovcharenko, G. N. Tolmachova, and P. N. Vygov, "High-Temperature Air Oxidation of E110 and Zr-1Nb Alloys Claddings with Coatings," *Problems of Atomic Science and Technology* 89 (2014): 126–132.
37. U. Wiklund, P. Hedenqvist, S. Hogmark, B. Stridh, and M. Arbell, "Multilayer Coatings as Corrosion Protection of Zircaloy," *Surface and Coatings Technology* 86–87 (1996): 530–534, [https://doi.org/10.1016/S0257-8972\(96\)03001-0](https://doi.org/10.1016/S0257-8972(96)03001-0)
38. D. Q. Peng, X. D. Bai, F. Pan, H. Sun, and B. S. Chen, "Influence of Aluminum Ions Implanted on Oxidation Behavior of ZIRLO Alloy at 500°C," *Vacuum* 80, no. 6 (2006): 530–536, <https://doi.org/10.1016/j.vacuum.2005.08.026>
39. U. D. Abdelrazek, S. W. Sharkawy, and H. A. El-Sayed, "Pyrolytic Carbon Coating of Zircaloy-4 Tubes at Relatively Low Temperatures," *Journal of Nuclear Materials* 249 (1997): 159–164, [https://doi.org/10.1016/S0022-3115\(97\)00214-6](https://doi.org/10.1016/S0022-3115(97)00214-6)
40. P. Ashcheulov, R. Škoda, J. Škarohlíd, A. Taylor, L. Fekete, F. Fendrych, R. Vega, et al., "Thin Polycrystalline Diamond Films Protecting Zirconium Alloys Surfaces: From Technology to Layer Analysis and Application in Nuclear Facilities," *Applied Surface Science* 359 (2015): 621–628, <https://doi.org/10.1016/j.apsusc.2015.10.117>
41. H.-G. Kim, I.-H. Kim, J.-Y. Park, and Y.-H. Koo, "Application of Coating Technology on Zirconium-Based Alloy to Decrease High-Temperature Oxidation," in *Zirconium in the Nuclear Industry: 17th International Symposium*, ed. R. J. Comstock and P. Barbéris (West Conshohocken, PA: ASTM International, 2014), 346–369, <https://doi.org/10.1520/STP15432012016>

42. J. R. Baczynski, "High Temperature Steam Oxidation of Titanium-Coated Zircaloy-2 and Titanium-Zirconium Alloys," (master's thesis, University of Illinois at Urbana-Champaign, 2014).
43. H. Yeom, B. Maier, R. Mariani, D. Bai, P. Xu, K. Sridharan, Y. Hwasung, et al., "Development of Zirconium-Silicide Coatings for Accident Tolerant Zirconium-Alloy Fuel Cladding," in *Proceedings of the International Congress on Advances in Nuclear Power Plants, ICAPP 2016* (LaGrange Park, IL: American Nuclear Society, 2016), 2126–2131.
44. J. C. Brachet, I. Idarraga-Trujillo, M. Le Flem, M. Le Saux, V. Vandenberghe, S. Urvoy, E. Rouesne, et al., "Early Studies on Cr-Coated Zircaloy-4 as Enhanced Accident Tolerant Nuclear Fuel Claddings for Light Water Reactors," *Journal of Nuclear Materials* 517 (2019): 268–285.
45. R. Van Nieuwenhove, V. Andersson, J. Balak, and B. Oberlander, "In-Pile Testing of CrN, TiAlN, and AlCrN Coatings on Zircaloy Cladding in the Halden Reactor," in *Zirconium in the Nuclear Industry: 18th International Symposium*, ed. R. Comstock and A. Motta (West Conshohocken, PA: ASTM International, 2018), 965–982, <https://doi.org/10.1520/STP159720160011>
46. S. PalDey and S. C. Deevi, "Single Layer and Multilayer Wear Resistant Coatings of (Ti, Al)N: A Review," *Materials Science and Engineering: A* 342, nos. 1–2 (2003): 58–79, [https://doi.org/10.1016/S0921-5093\(02\)00259-9](https://doi.org/10.1016/S0921-5093(02)00259-9)
47. M. Zhou, Y. Makino, M. Nose, and K. Nogi, "Phase Transition and Properties of Ti–Al–N Thin Films Prepared by R.F.-Plasma Assisted Magnetron Sputtering," *Thin Solid Films* 339, nos. 1–2 (1999): 203–208, [https://doi.org/10.1016/S0040-6090\(98\)01364-9](https://doi.org/10.1016/S0040-6090(98)01364-9)
48. A. Kimura, H. Hasegawa, K. Yamada, and T. Suzuki, "Metastable Ti1-xAlxN Films with Different Al Content," *Journal of Materials Science Letters* 9 (2000): 601–602.
49. T. Ikeda and S. Satoh, "Phase Formation and Characterization of Hard Coatings in the Ti–Al–N System Prepared by the Cathodic Arc Ion Plating Method," *Thin Solid Films* 195, nos. 1–2 (1991): 99–110, [https://doi.org/10.1016/0040-6090\(91\)90262-V](https://doi.org/10.1016/0040-6090(91)90262-V)
50. I. Younker and M. Fratoni, "Neutronic Evaluation of Coating and Cladding Materials for Accident Tolerant Fuels," *Progress in Nuclear Energy* 88 (2016): 10–18, <https://doi.org/10.1016/j.pnucene.2015.11.006>
51. M. Milosavljević, A. Grce, D. Peruško, M. Stojanović, J. Kovač, G. Dražič, A. Y. Didyk, and V. A. Skuratov, "A Comparison of Ar Ion Implantation and Swift Heavy Xe Ion Irradiation Effects on Immiscible AlN/TiN Multilayered Nanostructures," *Materials Chemistry and Physics* 133, nos. 2–3 (2012): 884–892, <https://doi.org/10.1016/j.matchemphys.2012.01.112>
52. M. Milosavljević, D. Peruško, V. Milinovic, Z. Stojanović, A. Zalar, J. Kovač, and C. Jaynes, "Ion Irradiation Stability of Multilayered AlN/TiN Nanocomposites," *Journal of Applied Physics D: Applied Physics* 43, no. 6 (2010), <https://doi.org/10.1088/0022-3727/43/6/O65302>
53. M. Milosavljević, M. Obradović, A. Grce, D. Peruško, D. Pjević, J. Kovač, G. Dražič, and C. Jaynes, "High Dose Ion Irradiation Effects on Immiscible AlN/TiN Nano-Scaled Multilayers," *Thin Solid Films* 544 (2013): 562–566, <https://doi.org/10.1016/j.tsf.2012.12.068>
54. M. Bugnet, T. Cabioch, V. Mauchamp, P. Guérin, M. Marteau, and M. Jaouen, "Stability of the Nitrogen-Deficient Ti₂AlN_x MAX Phase in Ar²⁺-Irradiated (Ti,Al)N/Ti₂AlN_x Multilayers," *Journal of Materials Science* 45 (2010): 5547–5552, <https://doi.org/10.1007/s10853-010-4615-0>
55. R. L. Boxman, D. M. Sanders, and P. J. Martin, ed., *Handbook of Vacuum Arc Science and Technology: Fundamentals and Applications* (Park Ridge, NJ: Noyes, 1995).
56. A. Anders, "Cathodic Arc Plasma Deposition," *Vacuum Technology, Coating & Hardware* 3 (2002): 1–26.

57. W. D. Sproul, "Physical Vapor Deposition Tool Coatings," *Surface and Coatings Technology* 81 (1996): 1–7, [https://doi.org/10.1016/0257-8972\(95\)02616-9](https://doi.org/10.1016/0257-8972(95)02616-9)
58. A. Wu, J. Ribis, J. C. Brachet, E. Clouet, F. Leprêtre, E. Bordas, and B. Arnal, "HRTEM and Chemical Study of an Ion-Irradiated Chromium/Zircaloy-4 Interface," *Journal of Nuclear Materials* 504 (2018): 289–299.
59. M. Ahlgren and H. Blomqvist, "Influence of Bias Variation on Residual Stress and Texture in TiAlN PVD Coatings," *Surface and Coatings Technology* 200 (2005): 157–160, <https://doi.org/10.1016/j.surfcoat.2005.02.078>
60. E. Lugscheider, C. Barimani, C. Wolff, S. Guerreiro, and G. Doepper, "Comparison of the Structure of PVD-Thin Films Deposited with Different Deposition Energies," *Surface and Coatings Technology* 86–87 (1996): 177–183.
61. K. L. Lin, M. Y. Hwang, and C. D. Wu, "The Deposition and Wear Properties of Cathodic Arc Plasma Deposition TiAlN Deposits," *Materials Chemistry and Physics* 46 (1996): 77–83, [https://doi.org/10.1016/0254-0584\(96\)80134-9](https://doi.org/10.1016/0254-0584(96)80134-9)
62. Y. Liu, I. Bhamji, P. J. Withers, D. E. Wolfe, A. T. Motta, and M. Preuss, "Evaluation of the Interfacial Shear Strength and Residual Stress of TiAlN Coating on ZIRLOTM Fuel Cladding using a Modified Shear-Lag Model Approach," *Journal of Nuclear Materials* 466 (2015): 718–727, <https://doi.org/10.1016/j.jnucmat.2015.06.003>
63. E. Alat, A. T. Motta, R. J. Comstock, J. M. Partezana, and D. E. Wolfe, "Ceramic Coating for Corrosion (C3) Resistance of Nuclear Fuel Cladding," *Surface and Coatings Technology* 281 (2015): 133–143, <https://doi.org/10.1016/j.surfcoat.2015.08.062>
64. E. Alat, A. T. Motta, R. J. Comstock, J. M. Partezana, and D. E. Wolfe, "Multilayer (TiN, TiAlN) Ceramic Coatings for Nuclear Fuel Cladding," *Journal of Nuclear Materials* 478 (2016): 236–244, <https://doi.org/10.1016/j.jnucmat.2016.05.021>
65. I. Younker and M. Fratoni, "Neutronic Evaluation of Coating and Cladding Materials for Accident Tolerant Fuels," *Progress in Nuclear Energy* 88 (2016): 10–18, <https://doi.org/10.1016/j.pnucene.2015.11.006>
66. *Standard Test Method for Adhesion Strength and Mechanical Failure Modes of Ceramic Coatings by Quantitative Single Point Scratch Testing*, ASTM C1624–05(2015) (West Conshohocken, PA: ASTM International, approved January 1, 2015): 1–29, <https://doi.org/10.1520/C1624-05R15.Scope>
67. M. Kirk, X. Yi, and M. Jenkins, "Characterization of Irradiation Defect Structures and Densities by Transmission Electron Microscopy," *Journal of Materials Research and Technology* 30, no. 9 (2015): 1195–1201, <https://doi.org/10.1557/jmr.2015.19>
68. R. E. Stoller, M. B. Toloczko, G. S. Was, A. G. Certain, S. Dwaraknath, and F. A. Garner, "On the Use of SRIM for Computing Radiation Damage Exposure," *Nuclear Instruments and Methods in Physics Research Section B: Beam Interactions with Materials and Atoms* 310 (2013): 75–80, <https://doi.org/10.1016/j.nimb.2013.05.008>
69. J. Ziegler, J. P. Biersack, and U. Littmark, *The Stopping and Range of Ions in Matter* (New York, NY: Pergamon Press, 1985).
70. H. Holleck, "Metastable Coatings—Prediction of Composition and Structure," *Surface and Coatings Technology* 36 (1988): 151–159, [https://doi.org/10.1016/0257-8972\(88\)90145-4](https://doi.org/10.1016/0257-8972(88)90145-4)
71. J. M. Andersson, J. Vetter, J. Müller, and J. Sjöln, "Structural Effects of Energy Input during Growth of Ti_{1-x}Al_xN (0.55 ≤ x ≤ 0.66) Coatings by Cathodic Arc Evaporation," *Surface and Coatings Technology* 240 (2014): 211–220, <https://doi.org/10.1016/j.surfcoat.2013.12.018>
72. S. PalDey and S. C. Deevi, "Properties of Single Layer and Gradient (Ti,Al)N Coatings," *Materials Science and Engineering: A* 361, nos. 1–2 (2003): 1–8, [https://doi.org/10.1016/S0921-5093\(03\)00473-8](https://doi.org/10.1016/S0921-5093(03)00473-8)
73. D. Wang, C. Chang, K. Wong, Y. Li, and W. Ho, "Improvement of the Interfacial Integrity of (Ti, Al) N Hard Coatings Deposited on High Speed Steel Cutting Tools," *Surface and Coatings Technology* 121 (1999): 388–394.

74. B. F. Coll, R. Fontana, A. Gates, and P. Sathrum, "(Ti-Al)N Advanced Films Prepared by Arc Process," *Materials Science and Engineering: A* 140 (1991): 816–824, [https://doi.org/10.1016/0921-5093\(91\)90519-S](https://doi.org/10.1016/0921-5093(91)90519-S)
75. P. J. Blau, "Scratch Adhesion Testing," in *Lab Handbook of Scratch Testing* (Oak Ridge, TN: Blue Rock Technical Publications, 2002), 7.1–7.15.
76. B. S. Xu, Y. X. Wu, H. D. Wang, Y. Jiang, and X. C. Zhang, "Hertzian Contact Response of Single-Layer, Functionally Graded and Sandwich Coatings," *Materials & Design* 28 (2005): 47–54, <https://doi.org/10.1016/j.matdes.2005.06.018>
77. F. Vaz, L. Rebouta, M. Andritschky, M. F. da Silva, and J. C. Soares, "Thermal Oxidation of $Ti_{1-x}Al_xN$ Coatings in Air," *Journal of the European Ceramic Society* 17 (1997): 1971–1977, [https://doi.org/10.1016/S0955-2219\(97\)00050-2](https://doi.org/10.1016/S0955-2219(97)00050-2)
78. H. Wang, R. Araujo, J. Swadener, Y. Wang, X. Zhang, E. Fu, and T. Cagin, "Ion Irradiation Effects in Nanocrystalline TiN Coatings," *Nuclear Instruments and Methods in Physics Research Section B: Beam Interactions with Materials and Atoms* 261, nos. 1–2 (2007): 1162–1166, <https://doi.org/10.1016/j.nimb.2007.04.248>
79. I. Kim, L. Jiao, F. Khatkhatay, M. S. Martin, J. Lee, L. Shao, X. Zhang, et al., "Size-Dependent Radiation Tolerance in Ion Irradiated TiN/AlN Nanolayer Films," *Journal of Nuclear Materials* 441, nos. 1–3 (2013): 47–53, <https://doi.org/10.1016/j.jnucmat.2013.05.035>
80. N. Norrby, "Microstructural Evolution of TiAlN Hard Coatings at Elevated Pressures and Temperatures" (PhD diss., Linköping University, 2014).
81. J. M. Castanho and M. T. Vieira, "Effect of Ductile Layers in Mechanical Behaviour of TiAlN Thin Coatings," *Journal of Materials Processing Technology* 143–144 (2003): 352–357, [https://doi.org/10.1016/S0924-0136\(03\)00454-0](https://doi.org/10.1016/S0924-0136(03)00454-0)
82. B. Borawski, J. A. Todd, J. Singh, and D. E. Wolfe, "The Influence of Ductile Interlayer Material on the Particle Erosion Resistance of Multilayered TiN Based Coatings," *Wear* 271 (2011): 2890–2898, <https://doi.org/10.1016/J.WEAR.2011.06.004>

Discussion

Question from Johannes Berstch, Paul Scherrer Institut:—Irradiation damage of the coating and the substrate develop differently. Does this lead to residual stress, maybe measurable with synchrotron radiation XRD?

Authors' Response:—This is an interesting question but one that we did not investigate as one would need to perform neutron irradiation on the bulk sample.

Questions from Mirco Grosse, KIT:

1. Do you plan on performing oxidation tests under accident conditions (LOCA, extended LOCA)?
2. Have you done or do you plan to do corrosion tests of bulk TiN and TiAlN for a better understanding of the dissolution behavior?

Authors' Response:

1. The project is finished and we do not plan any additional tests.
2. We only had a few tests at 500°C and 800°C. When the TiN layer was on the outer surface, we saw no evidence of dissolution.

Question from Marc Tupin, CEA:—Did you analyze the oxide formed at the surface of the multilayer coating during the corrosion process? As you know, aluminum oxide or hydroxide can be dissolved in water.

Authors' Response:—Yes, we are aware of that issue. As stated in the presentation, when TiN was the outer layer, no dissolution was observed. Also, oxidation in air at 1,000°C yielded mixed oxide phases of aluminum oxide, titanium oxide, and spinel formation based on the coating composition.

Question from Anand Garde, Zirashri, LLC:—In fuel loading, grid/fuel rod contact generates scratches on the fuel rod surface. Did you evaluate the effect of such surface damage on subsequent waterside corrosion?

Authors' Response:—In principle, our coating is harder than the grid, so that should not be an issue.

Question from Kit Coleman, ANT International:—During a LOCA or Fukushima-type accident one cannot avoid breaking the cladding; therefore, one needs to also protect the inside surface. Otherwise, the outside coating is a waste of effort.

Authors' Response:—In the case of an extended LOCA and station blackout, clearly it is not possible to totally avoid bad consequences, but stopping or slowing corrosion during the early part of the transient should provide some benefit and coping time.

Question from Bruce Kammenzind, Naval Nuclear Laboratory:—Due to the hydrogen over pressure used in the PWR (pressurized water reactor) primary coolant, the permeability of any coating to hydrogen is also an important property. It is only the oxide film forming on the zirconium alloy cladding surface that protects the zirconium alloy from direct adsorption of hydrogen. Can you comment on the permeability of the TiN/TiAlN coating to hydrogen?

Authors' Response:—Hydrogen permeability through TiN/TiAlN is several (three to four) orders of magnitude lower than in most metals, depending on the temperature. It has been shown that the hydrogen picked up during corrosion is the hydrogen generated in the corrosion reaction rather than hydrogen from hydrogen water chemistry, for example. This is always measured in the presence of a protective oxide layer, however.

Question from Peter Rudling, ANT International:—Current BWR (boiling water reactor) and PWR materials have excellent corrosion properties. How is this being addressed for ATF fuel development?

Authors' Response:—We agree that current materials have very good corrosion properties. Nevertheless, stopping corrosion and hydrogen pickup during normal operation and providing some additional coping time during an accident should be favorable. Whether it is worth the extra financial cost is something for fuel vendors and utilities to decide.

Question from Zoltan. Hozer, Hungarian Academy of Science:—When should the coatings be produced at an industrial scale? At the stage of capping tube production or after fuel rod production?

Authors' Response:—One of the advantages of the physical vapor deposition is that it is straightforward to scale it up to fuel rod size. It would most likely be easier to coat after fuel rod production but could also be performed after capping the tube.

Observation from Michael Preuss, University of Manchester:—This is a comment in response to Bertsch's question. Manchester carried out plenty of residual stress analysis on these coatings and we found very high compressive stresses after fabrication. But as the material is heated up to several 100°C, the stresses release very rapidly.

Authors' Response:—This is correct. We have no data on the stresses induced by irradiation damage, however.

Question from Rick Holt, Queen's University:—Have you considered the effect of thermal neutrons at high exposure on the chemical composition of the layers (via transmutation)?

Authors' Response:—We have not, unfortunately. This was only a three-year project.

Question from Guanze He, University of Oxford:—In this study, the radiation damage is investigated by in situ irradiation on a thin FIB sample. The large free surfaces of the FIB may suppress the diffusion process across the multilayer structure. So, how do you address the possible differences between the damage by in situ irradiation and what actually happened in service by neutrons?

Authors' Response:—The questioner is correct. The study of radiation damage in situ cannot be directly translated into an understanding of the behavior under neutron irradiation. It is possible, however, that if one can understand the physics of the radiation damage process that such experiments can provide valuable data for the neutron irradiation case.

Question from Yang-Pi Lin, GNF:—Please elaborate on the reason for the layered TiN/TiAlN architecture given that 1.5 μm of TiN provides protection. Why is a TiN monolith not sufficient?

Authors' Response:—The idea of the multilayer architecture was that the multiple layer-to-layer interfaces can help protect against crack propagation by deflecting or blunting the crack. This results in built-in damage tolerance. In addition, the rationale for incorporating the TiAlN into the design architecture is that it offers three to four orders of magnitude reduction in oxidation due to the lower oxygen permeability through the alumina outer layer as opposed to a titania oxide layer.